Available online at www.sciencedirect.com
ScienceDirect
Journal of the European Ceramic Society 30 (2010) 3407–3413
www.elsevier.com/locate/jeurceramsoc

Curvature and stresses for bi-layer functional ceramic materials

Jürgen Malzbender *

Forschungszentrum Jülich, IEF-2, 52425 Jülich, Germany

Received 19 May 2010; received in revised form 14 July 2010; accepted 24 July 2010
Available online 19 August 2010

Abstract

The technical application of layered functional ceramic components is challenged by curvature effects and residual stresses originating mostly from the thermal mismatch or chemical strains of the joined materials. Based on the general solution for elastic deformation of monolithic and multilayered materials the determination of curvature and residual stress for linear elastic bi-material specimens with chemical strains, chemical reduction in stiffness, shape variations, gradients in elastic modulus or thermal expansion is outlined. The use of the relationships is exemplified for ceramic solid oxide fuel cell (SOFC) and ceramic membrane materials. For SOFCs curvature changes are considered resulting from the reduction of the anode and crystallization of a glass–ceramic sealant with semi-spherical shape. For gas separation membranes which currently under development for fossil power plants the effect of chemical strains is assessed. The limits of using analytical relationships are addressed for the warpage of thin, rectangular SOFCs.

Keywords: Films; Mechanical properties; Residual stress; Membrane; Fuel cells

1. Introduction

Functional ceramic layers materials find widespread use in electronic, magnetic, optical, and structural components. Theories to relate stress, strain and curvature to the mechanical and thermal loading have been established for isotropic materials, bi-layered,[1] multilayered composites and materials with different stiffness in tension and compression.[2] The layers are usually rigidly bonded and differences in the thermo-elastic materials properties will result in residual stresses which can facilitate component fracture.[3] Such stresses arise from manufacturing, i.e. intrinsic stresses due co-firing, differences in thermal expansion, thermal/chemical gradients or phase changes.[4–6] Since the solutions usually concentrate on the simple cases the purpose of the present study is to give analytical solutions for more complex cases and to exemplify their use for functional ceramic materials.

Ceramic materials are used widely as anode, electrolyte and cathode[7] in SOFCs, which are highly efficient devices for converting chemical fuels directly into electrical energy. Especially the planar design has proven to be successful for stacks with high power density.[8] In the case of asymmetric designs and for unconstrained layered composites the residual stress is reflected as warping. In SOFC stacks the cells are connected in serial mode with intermediate bipolar plates via contact layers, hence curvature effects have to be eliminated during assembling for example by applying a permanent mechanical load. Operation of an SOFC stack at high temperatures (600–900 °C) obviously results in significant changes residual stress which for free cells will be reflected in a curvature change. A means to assess residual stresses is to measure the curvature of free components, where the stress state in the cell can be determined via a curvature measurement of the bi-layer composite anode–electrolyte.[4] In fact for SOFCs the curvature is also influenced by the oxidation state of the anode, i.e. it has been reported that the reduction of the anode leads to a significant increase in the curvature of the component.

The SOFC stack has to be gas tight, hence an inner sealant has to separate anode and cathode compartment and an outer sealant has to isolate the anode and cathode from the outer environment. Hence, the sealant material as well as the other stack components will be exposed to residual stresses due to difference in thermal expansion or crystallization strain, which again can be assessed using curvature measurements of for example sealant – steel substrate composites. Examples are presented for curvature and stress effects in SOFC materials due to the reduction of an anode and a crystallization of glass–ceramic sealant

* Tel.: +49 2461 61 6964; fax: +49 2461 61 3699.
E-mail address: j.malzbender@fz-juelich.de.

0955-2219/$ – see front matter © 2010 Elsevier Ltd. All rights reserved.
doi:10.1016/j.jeurceramsoc.2010.07.036

with semi-spherical shape. An outlook is given to a more complex case of geometrical non-linearity that requires the use of finite element calculation.

Global warming and the CO_2 problem has increased interest in perovskite ceramic oxides of ABO_3 type (rare earth metal ions on A sites, and transition metal ions on B sites) since they appear to be suited for potential applications in gas separation membranes.[9] When operated at high temperatures, these mixed ionic and electronic conducting perovskite membranes provide high oxygen permeation rates. Besides such advantageous functional performances the challenges of mechanical integrity especially in industrial applications need to be considered to prevent the mechanical failure of the membranes during exposure at elevated temperatures and thermal cycles, but also to avoid fracture caused by a large chemical gradient of oxygen and resulting chemical strains of 0.2% to 0.4%.[10,11] Hence an example is given how the effect of chemical strains can be assessed for layered gas separation membranes which exhibit chemical strain behavior.

1.1. General theory and outlook

Suppose an elastic multilayer composite where n layers (thicknesses t_j) are bonded. The subscript, j, denotes the layer number ranging from 1 to n.[12] The coordinate system is defined such that the surface of the layer 1 is located at $z=0$. The applied forces and moments can be linked to the stresses using Euler–Bernoulli beam theory.[13] Hence, the resultants of the axial force N, shear force Q and the bending moment M are related to the axial normal σ_x and transverse shear stress $\tau_{x,y}$ as:

$$N + N_\alpha = w \int_0^{t_n} \sigma_x dz \tag{1}$$

$$M + M_\alpha = w \int_0^{t_n} \sigma_x z dz \tag{2}$$

$$Q = w \int_0^{t_n} \tau_{x,y} dz \tag{3}$$

where z is the position relative to the surface and N_α and M_α are the axial force and bending moment acting on the layers $j=1$ to n due to the difference in thermal or isothermal expansion. The parameter w is the width of the beam. In general M, N and Q can be a function of the in-plane position x. At the position z perpendicular to the interface between the layers the strain $\varepsilon_{x,j,z}$ and stress $\sigma_{x,j,z}$ in the layer j are[13]:

$$\varepsilon_{x,j,z} = \varepsilon_{x,0} + z\kappa - \int_{T_{0,j}}^{T_{1,j}} \alpha_j(T,z) dT(z) \tag{4}$$

$$\sigma_{x,j,z} = \overline{E_j} \left(\varepsilon_{x,0} + z\kappa - \int_{T_{0,j}}^{T_{1,j}} \alpha_j(T,z) dT(z) \right) \tag{5}$$

where $\varepsilon_{x,0}$ is the strain the at $z=0$ and κ the curvature of the beam. In the case of a two dimensional geometry the biaxial elastic modulus is given by $\overline{E} = E/(1-\nu^2)$. The parameter α represents the thermal expansion coefficient, which can be a function of z and the temperature T. The temperature $T_{0,j}$ is the initial and $T_{1,j}$ the final temperature in the layer j. The current approach can be extended to non-negligible shear stresses.[13] The resulting relationships between the force, moment and beam deformation are

$$\begin{Bmatrix} N + N_\alpha \\ M + M_\alpha \end{Bmatrix} = \begin{bmatrix} A & B \\ B & D \end{bmatrix} \begin{Bmatrix} \varepsilon_{x,0} \\ \kappa \end{Bmatrix} \tag{6}$$

where the symbols A, B and D denote the extensional, flexural-extensional coupling and flexural stiffness coefficients.[12] Note that these equations take the temperature dependency of the stiffness into consideration as well as the effect of temperature gradients within the layers.

The case of a linear proportionality of thickness and temperature $dT = \Delta T = T_0 + z\,T^*$ has been outlined before.[12] If the plate like layered composite is constrained at its edges by an elastic material (sealant) A has to be substituted by $A + E_{\text{seal}}\ l/2\ t$ and D by $D + E_{\text{seal}}\ l/2\ t^2$, due to the changed boundary conditions.[14] Here E_{seal} is the stiffness of the sealant, l is the plate width and $t = \sum_{i=1}^{n} t_i$ the plate height.

The thermal or isothermal expansion of bi-layers can be assessed by curvature measurements. For more complex multilayered materials multiple measurements of composites with increasing number of layers might be necessary. A direct assessment of residual stress might be possible by for example X-ray diffraction or the hole drilling method, requiring minimum stress levels of ~30–50 MPa. A recent variation of the hole drilling method for μm thin layers is based on the cutting of a notch using a focused ion beam, requiring even higher stress of the order of hundreds of MPa.[15] In order to assess the reliability the residual stress has to be compared to the strength of the material, where for brittle materials statistical aspects of failure probability have to be considered. Note that such statistics obtained from testing of isotropic specimens might not be valid to predict the failure of thin layers since the defect size will be limited by the layer thickness.[16]

1.2. Special theory for bi-layered materials and outlook

Due to their technical relevance and assessment simplification of the mechanical behaviour of functional ceramic composites only bi-layer materials are considered in the following. Obviously the number of unknown parameters and uncertainty increase with the number of layers in a composite where especially the problems associated with the thickness measurement of a thin layer can lead to large uncertainties. Special consideration is given to the effect of a change in substrate stiffness (reduction of a SOFC anode), effect of phase changes (crystallisation of a glass–ceramic sealant) and chemical strain (gas separation membrane).

For the special case of a bi-layer material first the general solution for layers of equal width is given, which permits also an assessment of the effect of an isothermal change in substrate stiffness (reduction). Then consideration is given to the cases where substrate and coating have a width that decreases with the distance from the interface. This is an effect typically observed for glasses and glass–ceramics deposited on a sub-

Table 1
Relationships for curvature and strain.

$\Delta\kappa$	$\varepsilon_{x,0}$	Remark
(7) $\frac{6A_1A_2(1+A_2)(\varepsilon_C-\varepsilon_S)}{(1+A_1A_2(4A_2(6+A_2(4+A_1A_2))))t_S}$	(8) $\frac{\varepsilon_S+A_1A_2((-2-3A_2+A_1A_2^3)\varepsilon_C+(6+A_2(9+4A_2))\varepsilon_S)}{(1+A_1A_2(4A_2(6+A_2(4+A_1A_2))))}$	Both layers with equal width
(9) $\frac{6A_1A_2(3+2A_2)(\varepsilon_C-\varepsilon_S)}{(6+A_1^2A_2^4+6A_1A_2(2+A_2(2+A_2)))t_S}$	(10) $\frac{6\varepsilon_S+A_1A_2((-6-6A_2+A_1A_2^3)\varepsilon_C+6(3+A_2(3+A_2))\varepsilon_S)}{(6+A_1^2A_2^4+6A_1A_2(2+A_2(2+A_2)))}$	Semi-triangular shape coating on rectangular substrate
(11) $\frac{12A_1A_2(3+2A_2)(\varepsilon_C-\varepsilon_S)}{(24+A_1^2A_2^4+12A_1A_2(2+A_2(2+A_2)))t_S}$	(12) $\frac{A_1^2A_2^4\varepsilon_C+24\varepsilon_S+12A_1A_2(-(1+A_2)\varepsilon_C+(3+A_2(3+A_2))\varepsilon_S)}{(24+A_1^2A_2^4+12A_1A_2(2+A_2(2+A_2)))}$	Semicircular shape coating on rectangular substrate
(13) $\frac{6A_1A_2(1+A_2)(\varepsilon_C-\varepsilon_S)}{(1+A_1A_2(3+A_2(4+A_2(3+A_1A_2))))t_S}$	(14) $\frac{\varepsilon_S+A_1A_2((-3-4A_2+A_1A_2^3)\varepsilon_C+(6+A_2(8+3A_2))\varepsilon_S)}{1+A_1A_2(3+A_2(4+A_2(3+A_1A_2)))}$	Coating and substrate semi-triangular or cylindrical
(15) $\frac{A_1A_2(3+A_2(4+A_1A_2))\varepsilon_{\max}}{(1+A_1A_2(4+A_2(6+A_2(4+A_1A_2))))t_S}$	(16) $\frac{A_1A_2(1+A_2(2+A_1A_2))\varepsilon_{\max}}{1+A_1A_2(4+A_2(6+A_2(4+A_1A_2)))}$	Coating induces isothermal strain with max. value in surface
(17) $\frac{\varepsilon_{\max S}+A_1A_2((3+A_2(4+A_1A_2))\varepsilon_{\max C}-(2+3A_2)\varepsilon_{\max S}}{(1+A_1A_2(4+A_2(6+A_2(4+A_1A_2))))t_S}$	(18) $\frac{A_1A_2(-(1+A_2(2+A_1A_2))\varepsilon_{\max C}+2(1+A_2)^2\varepsilon_{\max S}}{1+A_1A_2(4+A_2(6+A_2(4+A_1A_2)))}$	Coating and substrate induce isoth. strain max. value in surface
(19) $\frac{A_1A_2(3+A_2(2-A_1A_2))\varepsilon_{\max}}{(1+A_1A_2(4+A_2(6+A_2(4+A_1A_2))))t_S}$	(20) $\frac{A_1A_2(1+A_2(-1+A_1A_2^2))\varepsilon_{\max}}{1+A_1A_2(4+A_2(6+A_2(4+A_1A_2)))}$	Coating induces isothermal strain with max. value in interface
(21) $-\frac{\varepsilon_{\max S}+A_1A_2((-3+A_2(-2+A_1A_2))\varepsilon_{\max C}+(4+3A_2)\varepsilon_{\max S}}{(1+A_1A_2(4+A_2(6+A_2(4+A_1A_2))))t_S}$	(22) $\frac{\varepsilon_{\max S}+A_1A_2((1+A_2)(-1+A_1A_2^2))\varepsilon_{\max C}+(4+A_2(5+2A_2))\varepsilon_{\max S}}{1+A_1A_2(4+A_2(6+A_2(4+A_1A_2)))}$	Coating and substrate induce isoth. strain max. value in interface

strate and associated with the surface wetting of the material. Finally the relationships to assess the effect of chemical strains are given.

In the case of thermal expansion related effects the substrate strains ε_S has to be substituted by $\alpha_S \cdot T$ and the coating strain ε_C by $\alpha_C \cdot T$. A measurement of the curvature change permits therefore a calculation of the strain in the coating. The general relationships for curvature and strain at the free surface $z=0$ of a bi-layer specimen with layers of equal width are given in Table 1, Eqs. (7) and (8), where for simplification the normalisation $A_1 = E_C/E_S$ and $A_2 = t_C/t_S$ are used.

Due to the deposition process, the width of the coating might change as a function of height. Examples of possible shapes are illustrated in Fig. 1. Assuming a semi-triangular shape, with w being the width of the substrate, the width of the coating can be related to the position (z) relative to the interface as $w_C = w(1-(z-t_S)/t_C)$. The resulting relationships for curvature and strain are given in Table 1 as Eqs. (9) and (10). Assuming a semi-cylindrical shape (Fig. 1), the width of the coating can be related to the position (z) relative to the interface as $w_C = w\sqrt{1-(z-t_S)/t_C}$ then the relationships for the curvature and strain change into Eqs. (11) and (12) in Table 1.[6]

If coating and substrate have a semi-triangular shape, the width of the coating can be related to the position (z) relative to the interface as $w_C = w_{\max}(1-(z-t_S)/t_C)$. With the width of the substrate $w_S = w_{\max}(1-(-z+t_S)/t_S)$ (Fig. 1) the relationships for curvature and strain can be written in the form of Eqs. (13) and (14) in Table 1. Finally, assuming a semi-cylindrical shape of coating and substrate (Fig. 1), the width of the coating can be related to the position (z) relative to the interface as $w_C = w_{\max}\sqrt{1-(z-t_S)/t_C}$, of the substrate $w_C = w_{\max}\sqrt{1-(-z+t_S)/t_S}$. The resulting relationships are identical to Eqs. (13) and (14).

Fig. 1. Schematic of some specimen geometries.

The thermo-mechanical load might also be a result of isothermal/chemical strain. Assuming a chemically strained layer on an inert substrate ($\varepsilon_S = 0$), the strain in the layer might change linear with thickness $\varepsilon_C = ((z-t_S)/t_C)\varepsilon_{\max}$. Hence curvature and strain are represented by Eqs. (15) and (16) in Table 1. In a more complex case the support might not be inert, with $\varepsilon_C = ((z-t_S)/t_C)\varepsilon_{\max C}$ and $\varepsilon_S = (z/t_S)\varepsilon_{\max S}$, the curvature and the strain are given by Eqs. (17) and (18) in Table 1. However, alternatively the free surface of the chemically strained layer might also be at strain zero. If the substrate is inert ($\varepsilon_S = 0$) and the strain in the layer changes linear with thickness $\varepsilon_C = (1-(z-t_S)/t_C)\varepsilon_{\max}$ the equations become to (19) and (20) in Table 1. Finally, both support and materials exhibit chemical strains, $\varepsilon_C = (1-(z-t_S)/t_C)\varepsilon_{\max C}$ and $\varepsilon_S = (1-z/t_S)\varepsilon_{\max S}$, the relationships for curvature and strain become Eqs. (23) and (24) in Table 1.

The analysis of non-elastic effects is not the aim of the current analysis. However, solution or bi-materials are available in the literature to consider the effect of plasticity[17,18] creep[19,20] and viscoelasticity[21] or the interaction of creep deformation and scale growth processes.[22] In particular creep can lead to failure due to expansion of a creep damage zone from the tensile surface.

2. Case studies

Example A: an example for the use of the relationships is the curvature change due to a stiffness change in the case of a reduction of the NiO to Ni. The substrate in an as-produced anode

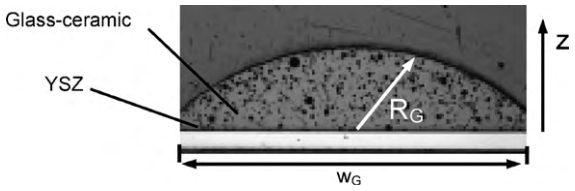

Fig. 2. Cross-section view of glass–ceramic/YSZ specimen.

supported SOFC typically contains NiO and YSZ. Typically in such a functional ceramic component an YSZ electrolyte layer is deposited on a porous NiO/YSZ composite substrate and then co-fired. The NiO in the composite substrate has to be reduced to Ni at a temperature that is lower than the co-firing temperature before operation to provide the necessary functionality.

A bi-layer YSZ electrolyte on the Ni/YSZ cermet shows a curvature change compared to a bi-layer YSZ electrolyte on the NiO/YSZ substrate. The CTE of NiO/YSZ is different from the CTE of Ni/YSZ, however, since an isothermal effect is considered which has been observed in situ at elevated temperatures[24] the CTE change cannot be responsible for the reported curvature change. Note that the reduction process is not associated with a chemical expansion/shrinkage of the NiO to Ni in the substrate[23]; hence the change in curvature can be associated with the lower stiffness of the Ni/YSZ substrate.[24] Typically the stiffness of the electrolyte (10 μm) is ∼200 GPa, the value for the substrate (1 mm) before reduction ∼100 GPa and ∼50 GPa after reduction.[24] Hence using Eqs. (7) and (8) an increase in curvature of ∼3.3 is obtained, whereas the stress will change only by ∼10%. In fact, similar values for the curvature changes have been reported in the literature.[25]

Example B: an example for an entirely geometrical anisotropy for a bi-layer is the effect of a change of the width of glass–ceramic sealants which is applied on top of a substrate similar to the sealants used for SOFC stacks. Here the width decreases with distance from the interface due to wetting effects. In order to assess the properties the material can be deposited on either an YSZ or steel substrate, contrary to the application in a SOFC stack where the material is in a sandwich between either YSZ and steel or between two steel plates. The deposition of on a single substrate permits to assess the difference in thermal and isothermal expansion via curvature measurements. Such differences have been reported for sealants deposited on steel as compared to YSZ substrates, where the differences between the behaviour of the bi-layers have partly been associated with the creep of steel at elevated temperatures.[26] The sealants showed typically a semicircular shape (Fig. 2). The observed change in curvature during a dwell time at high temperatures (see Fig. 3) was considered to be the result of the sealant crystallisation of the glass to become a glass–ceramic composite. Assuming a purely crystallisation induced strain ε_C ($\varepsilon_S = 0$) and based on the relationships (11) and (12) and the material properties given in[26] it can be determined that the strain increases with progressive crystallisation up to 0.05%.

Example C: perovskites used for gas separation are known to exhibit an oxygen partial pressure dependent change in lattice parameter. Since the membrane operation requires an oxygen

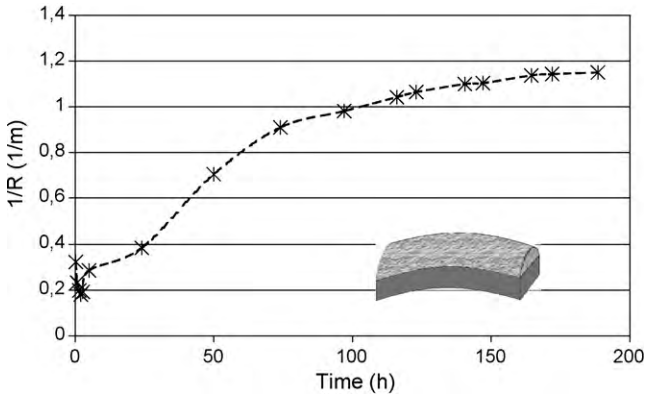

Fig. 3. Isothermal curvature change of glass–ceramic A on YSZ at 850 °C.

gradient, chemical strains arise across the thickness. They have to be assessed to estimate the failure probability of the perovskite under operation. In order to increase the permeation the membrane layer might need to be very thin and hence supported by a porous substrate in practical application.

Since the material will shrink under lower oxygen partial pressure (vacuum) the maximum strain ε_{max} will arise where the oxygen partial pressure is lowest, which can depending on the set-up either be at the free surface of the membrane or at the interface to the substrate. It is reasonable to assume that the stiffness of the porous substrate is 100 GPa, the value of the membrane 200 GPa and the chemical strain in the membrane increases roughly linear with thickness with a maximum value of ∼0.2% at the free surface of the membrane on an inert substrate (Table 2).[10,11]

The data presented in Table 2 illustrate that the compressive strain in the membrane decreases as the substrate thickness increases, leading to tensile stresses near the interface to the substrate. However, the tensile strain is still lower than the value of 0.1% that would develop for a free membrane. In addition the tensile stress in the substrate becomes larger as the membrane thickness decreases which eventually can cause failure of this support. Using a sealant to clamp the edges reduces the tensile stress in the membrane and the maximum stress in the support. Note that, whereas the remaining deflection for a plate length of 0.1 m is less than 0.5 μm, it is ∼30 μm for a plate of 1 m length.

Example D: the examples presented above are limited to quadratic or circular specimens where the substrate thickness is significantly larger than the coating thickness since then the components have a spherical shape.[27] When the substrate thickness is reduced a bifurcation arises with different curvatures in both in-plane directions and the component will display a

Table 2
Strain (%) in supported membranes.

Substrate thickness/mm	Substrate–free surface (thickness 50 μm)	Interface	Membrane–free surface
1	−0.005	0.01	−0.19
0.5	−0.01	0.02	−0.18
0.25	−0.02	0.03	−0.16
0.25 – edges clamped	0.005	0.005	−0.195

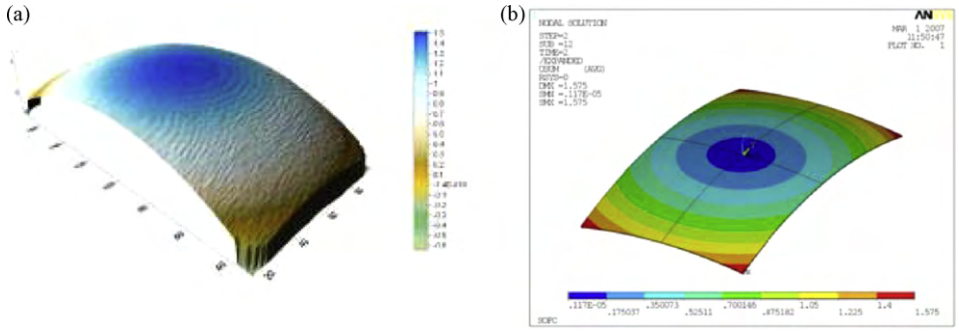

Fig. 4. Experimental (a) and simulated (b) deformation of a cell with a 465 μm thick anode substrate.

cylindrical shape. Results from laminated piezoelectric materials demonstrated that the larger the difference between the two in-plane lengths for a bi-layered composite the stronger the difference between the two in-plane curvatures.[28] In order to gain insight into the warping behaviour in the case of large deflection and the effect of a rectangular geometry the complex curvature of anode supported SOFCs has been studied using the finite element simulation package ANSYS (typically 900 shell elements were used in a simulation). In fact stacks with rectangular cell geometry have proven to be advantageous for the fast heating requirements in auxiliary power units.[29]

Typical measured curvature profiles for cells (in-plane ~8.5 cm × 15 cm) with a 465 μm and 300 μm anodes substrates as measured using a laser profilometer are shown in Figs. 4a and 5a, respectively. For details on the processing of such SOFC cells see,[30] for the elastic moduli and thermal expansion coefficients see.[3] The anode substrate supports a ~8 μm thick YSZ electrolyte. The cell with the thicker anode possesses a spherical curvature the cell with the thinner anode substrates has a cylindrical shape. The maximum deflection of the cells is 1.49 ± 0.06 mm and 1.75 ± 0.10 mm for the cell with 300 μm and 465 μm thick anode substrate, respectively.

The measured curvature of the thicker cell compares well with the simulated linear material deformation (Fig. 4b). Note that for the thinner cell non-linear geometric effects have to be explicitly considered in the simulation. This non-linear simulation with no initial curvature leads to a cylindrical shape in the opposite direction of the experimental observation (Fig. 5b). However, the result of the non-linear simulation agrees with the experimental simulation, if the cell has a small initial curvature in the short direction (radius 20 m) or if a small anisotropy in the elastic moduli (~10%) or thermal expansion coefficient in *x*- and *y*-direction is considered (~2%).

Although it was not possible to verify such small effects experimentally, anisotropic materials properties are not unusual in such tape casted products. In fact, although the terms spherical and cylindrical curvature are used in the manuscript for simplification a detailed look at the shape of the specimens revealed that

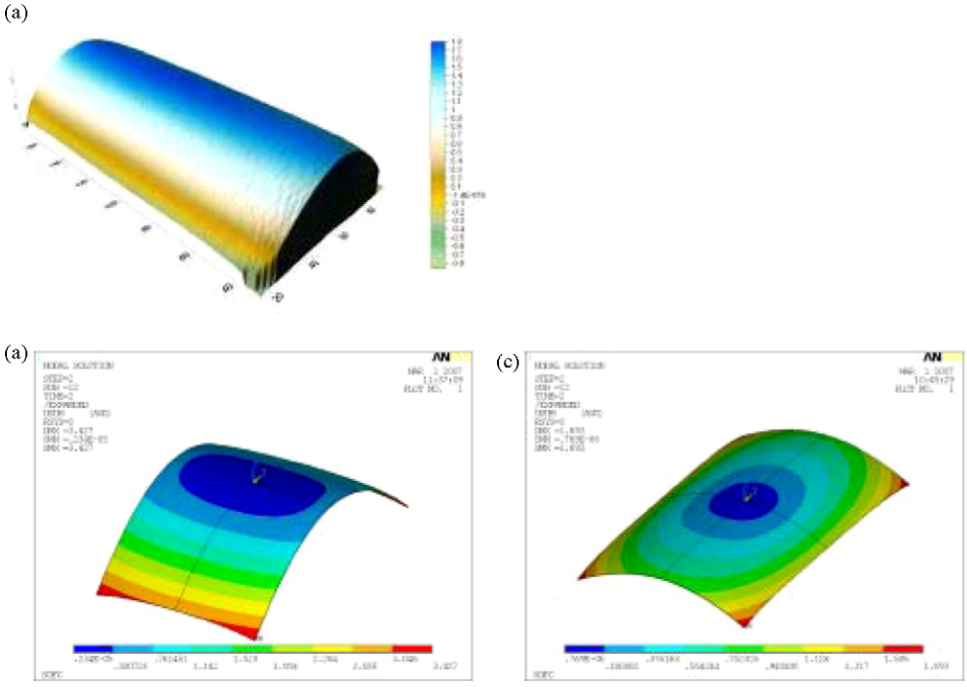

Fig. 5. Experimental (a) and simulated (b, c) deformation of a cell with a 300 μm thick anode substrate.

the cylindrical curvature is rather a parabolic curvature and the spherical curvature is a superposition of parabolic curvatures in both in-plane directions.

The electrolyte and thick anode substrate residual stress which result from the mismatch in thermal expansion are nearly independent of the in-plane direction with values of ∼−310 MPa and 21 MPa, respectively. As to be expected, for the thinner component the anode stress increases by 50% whereas the electrolyte stress decreases only by 10%.

Further simulations, not given here in detail, have been carried out with the aim to determine the critical parameter for the change in shape and revealed that for the current rectangular shaped cells the shape changes from spherical to cylindrical requires an anode substrate thickness of ∼400 μm. Considering the side length ratio of the cylindrical cell of 1.7 given above a change from spherical to cylindrical shape occurs for a cell of ∼62 mm × 106 mm for an anode substrate thickness of 300 μm and ∼100 mm × 176 mm for an anode substrate thickness of 465 μm, i.e. it can be concluded that the thicker the anode substrate the larger is the side length ratio at which the change from spherical to cylindrical curvature occurs.

Additional simulations have also shown that a change from spherical to cylindrical geometry occurs at a side length of ∼80 mm for a square cell with an anode substrate thickness of 300 μm with the slight anisotropy in elastic modulus or thermal expansion coefficient defined above. For a cell with an anode substrate thickness of 465 μm this change occurs if a side length of ∼130 mm is exceeded. This implies that the shape in change occurs once a critical surface area has been exceeded.

3. Conclusions

Relationships have been derived for curvature and residual stress of linear elastic bi-material specimens with chemical strains, chemical reduction in stiffness, shape variations, gradients in elastic modulus or thermal expansion. The use of the relationships has been illustrated for the SOFC curvature change resulting from the reduction of the anode yielding values which agree well with literature and a glass–ceramic sealant with semi-spherical shape where the interestingly the crystallization leads to curvature changes and strains. For gas separation membranes currently under development for fossil power plants the effect of chemical strains has been addressed considering the effect of the geometrical arrangement with respect to the surrounding atmosphere and sealant. The limits with respect to thickness of using analytical relationships are addressed for the warpage of thin, rectangular SOFCs.

Acknowledgements

The author would like to thank Dr. J. Ruska, Dr. J. Ernst and Dr. S. Stolz (CeramTec AG, Marktredwitz, Germany) for providing the rectangular half-cells for curvature measurements carried out by Dr. M. Bram (IEF-1). The finite element simulations were supported by Dr. J. Wolters (ZAT). The work was partly financially supported by the Mem-Oxycoal project (BMWi funding number 0327803D).

References

1. Roark RJ, Young WC. *Formulas for stress and strain*. Singapore: McGraw-Hill; 1984.
2. Malzbender J, Steinbrech RW. Determination of the stress-dependent stiffness of plasma-sprayed thermal barrier coatings using depth-sensitive indentation. *J Mater Res* 2003;**18**:1975–84.
3. Malzbender J, Steinbrech RW, Batfalsky P. Fracture energies of brittle sealanats for planar solid oxide fuel cells. *Ceram Eng Sci Proc* 2005;**26/4**:191–285.
4. Fischer W, Malzbender J, Steinbrech RW. Studies of residual stresses in planar solid oxide fuel cells. *J Power Sources* 2008;**182**:594–8.
5. Hendriksen PV, Carter DJ, Mogensen M. Dimensional instability of doped lanthanum chromites in an oxygen pressure gradient. *Proc Electrochem Soc* 1995;**951**:934–43.
6. Adamson MT, Travis RP. Comparison of stress generation mechanism in a planar solid oxide fuel cell stack. *Proc Electrochem Soc* 1997;**18**: 691–9.
7. Tietz F. Thermal expansion of SOFC materials. *Ionics* 1999;**5**:129–39.
8. Blum L, Meulenberg WA, Nabielek H, Steinberger-Wilckens R. Worldwide SOFC technology overview and benchmark. *Int J Appl Ceram Technol* 2005;**2**:482–92.
9. Sunarso J, Baumann S, Serra JM, Meulenberg WA, Liu S, Lin YS, Diniz da Costa JC. Mixed ionic-electronic conducting (MIEC) ceramic-based membranes for oxygen separation. *J Membr Sci* 2008;**320**:13–41.
10. McIntosh S, Vente JF, Haije WG, Blank DHA, Bouwmeester HJM. Oxygen stoichiometry and chemical expansion of $Ba_{0.5}Sr_{0.5}Co_{0.8}Fe_{0.2}O_{3-\delta}$ measured by in situ neutron diffraction. *Chem Mater* 2006;**18**: 2187–93.
11. Lein HL, Wiik K, Grande T. Thermal and chemical expansion of mixed conducting $La_{0.5}Sr_{0.5}Fe_{1-x}Co_xO_{3-\delta}$ materials. *Solid State Ionics* 2006;**177**:1795–8.
12. Malzbender J. Mechanical and thermal stresses in multilayered materials. *J Appl Phys* 2004;**95**:1780–2.
13. Tran AD, Bert CW. Bending of thick beams of bimodulus materials. *Comput Struct* 1982;**15**:627–42.
14. Qu J.*Conference proceedings, SECA core technology program review meeting*. NETL Publications; 2003.
15. Malzbender J, Steinbrech RW, Singheiser L. A review of advanced techniques for characterising SOFC behavior. *Fuel Cells* 2009;**9**:785–93.
16. Malzbender J, Steinbrech RW. Threshold fracture stress of thin ceramic components. *J Eur Ceram Soc* 2008;**28**:247–52.
17. Hu YY, Huang WM. Elastic and elastic–plastic analysis of multilayer thin films: closed-form solutions. *J Appl Phys* 2004;**96**:4154–60.
18. Zhang XC, Xu BS, Xuan FZ. Residual stresses in the elastoplastic multilayer thin film structures: the cases of Si/Al bilayer and Si/Al/SiO_2 trilayer structures. *J Appl Phys* 2008;**103**:073505.
19. Zhang XC, Xu BS, Wang HD, Wu YX. Residual stress relaxation in the film/substrate system due to creep deformation. *J Appl Phys* 2007;**101**:083530.
20. Cen Q-Q, Xuan FZ, Tu S-T. Modeling of creep deformation and its effect on stress distribution in multilayer systems under residual stress and external bending. *Thin Solid Films* 2009;**517**:2924–9.
21. Chang W-J, Fang T-H, Weng C-I. Thermoviscoelastic stresses in thin films/substrate system. *Thin Solid Films* 2007;**515**:3693–7.
22. Limarga AM, Wilkinson DS. Modeling the interaction between creep deformation and scale growth process. *Acta Mater* 2007;**55**:189–201.
23. Ivers-Tiffée E, Timmermann H, Leonide A, Menzler NH, Malzbender J. Methane reforming kinetics, carbon deposition, and redox durability of Ni/8 yttria-stabilized zirconia (YSZ) anodes. In: Vielstich W, Yokokawa H, Gasteiger HA, editors. *Handbook of fuel cells*, vols. 5–6. Wiley; 2009. p. 933–56.
24. Malzbender J, Steinbrech RW, Singheiser L. Failure probability of solid oxide fuel cells. *Ceram Eng Sci Proc* 2005:293–7, 26/4.
25. Sun B, Rudkin RA, Atkinson A. Effect of thermal cycling on residual stress and curvature of anode-supported SOFCs. *Fuel Cells* 2009;**9**:805–13.

26. Malzbender J, Koppitz T, Gross SM, Steinbrech RW. Studies on the thermal expansion of glass–ceramic sealants. *Proc 7th Eur SOFC Forum* 2006:P0418.
27. Salamon NJ, Masters CB. Bifurcation in isotropic thinfilm/substrate plates. *Int J Solids Struct* 1995;**32**:473–81.
28. Hyer MW, Jilani A. Predicting the deformation characteristics of rectangular unsymmetrically laminated piezoelectric materials. *Smart Mater Struct* 1998;**7**:784–91.
29. Gubner A, Nguyen-Xuan T, Bram M, Remmel J, de Haart LGJ. Lightweight cassette type SOFC stacks for automotive applications. *Proc 7th Eur SOFC Forum* 2006:42.
30. Menzler NH, Buchkremer HP, Ernst J, Kauert R, Ruska J, Stöver D, Stolz S. Manufacturing of solid oxide fuel cells – bridging the gap from laboratory to industry. *Mater Sci Forum* 2007;**539–543**:1315–20.